Progress In Electromagnetics Research, Vol. 142, 437–462, 2013

DIPOLE RADIATION NEAR ANISOTROPIC LOW-PERMITTIVITY MEDIA

Mohammad Memarian* **and George V. Eleftheriades**

The Edward S. Rogers Sr. Department of Electrical and Computer Engineering, University of Toronto, 40 St. George Street, Toronto, Ontario M5S 2E4, Canada

Abstract—We investigate radiation of a dipole at or below the interface of (an)isotropic Epsilon Near Zero (ENZ) media, akin to the classic problem of a dipole above a dielectric half-space. To this end, the radiation patterns of dipoles at the interface of air and a general anisotropic medium (or immersed inside the medium) are derived using the Lorentz reciprocity method. By using an ENZ half-space, air takes on the role of the denser medium. Thus we obtain shaped radiation patterns in air which were only previously attainable inside the dielectric half-space. We then follow the early work of Collin on anisotropic artificial dielectrics which readily enables the implementation of practical anisotropic ENZs by simply stacking sub-wavelength periodic bi-layers of metal and dielectric at optical frequencies. We show that when such a realistic anisotropic ENZ has a low longitudinal permittivity, the desired shaped radiation patterns are achieved in air. In such cases the radiation is also much stronger in air than in the ENZ media, as air is the denser medium. Moreover, we investigate the subtle differences of the dipolar patterns when the anisotropic ENZ dispersion is either elliptic or hyperbolic.

1. INTRODUCTION

The radiation of antennas at the interface of media has been the subject of numerous studies to date [1–13]. The scenario of interest is a classic problem in electromagnetics dating back to the work of Sommerfeld in 1909, investigating the radiation of a source above a lossy half-space [1]. For instance in [12] the radiation of dipoles placed on an air-dielectric interface was studied and it was found that the radiation

Received 8 August 2013, Accepted 2 September 2013, Scheduled 11 September 2013

* Corresponding author: Mohammad Memarian (m.memarian@mail.utoronto.ca).

Invited paper dedicated to the memory of Robert E. Collin.

mainly occurs inside the dielectric with interesting radiation pattern shapes. The radiation pattern in the air-side primarily had a single lobe, and more importantly, it was much weaker than the radiation in the dielectric, with an approximate power ratio of $1 : \epsilon^{3/2}$ [9]. Ref. [3] studied the problem of a dipole at the interface of an anisotropic plasma interface. Ref. [11] investigated the radiation patterns of both horizontal and vertical interfacial dipoles, deducing the location of the nulls and power ratios in either half-spaces. Other effects such as subsurface peaking was also explored by the same authors in [14]. Such studies have been intended for various applications such as Ground Penetrating Radar [15, 16], antennas for communication above earth or under water [2, 13], antennas on semiconductors [9] or above dielectrics for imaging [12], to only name a few.

Different techniques have been used thus far for analyzing this problem, mainly developing the Green's function and using asymptotic approximations to find the far-field radiation patterns inside the air or the dielectric regions. A great body of literature to date has been dedicated to solving the Sommerfeld type integrals that arise in these problems, (e.g., see [10] for a review of various works). The poor convergence of Sommerfeld type integrals has been an important reason for devising various efficient techniques for solving these types of problems as done in [17] and using integral equations solved with the Method of Moments [18, 19], and exact solutions such as [20]. Finite Difference Time Domain (FDTD) methods have also been used to analyze radiation patterns of such scenarios [16, 21], analyzing both the near-field [21] and the far-field [16, 21], pointing out some ripple effects on the patterns obtained due to finite observation distances. Effects of lateral waves were also explored in works such as [16, 22, 23]. Other time domain techniques have also been used for solving the problem of a source above a lossy half-space as in [24]. Furthermore, a few studies have investigated radiation from anisotropic media [3, 4, 25, 26] mainly through developing the Green's function of their scenario of interest.

Metamaterials (MTMs) — materials with constitutive parameters not usually found in nature — have received significant attention for more than a decade now and have found various applications in optics and electromagnetics. One type of MTMs relevant to this study are the Epsilon Near Zero (ENZ) media, which have shown interesting properties such as tailoring the phase of the radiation pattern of arbitrary sources [27]. Such materials are in contrast to normal dielectrics, which have permittivity values above the free space permittivity ϵ_0.

In almost all the work to date such as [9, 11, 12], the study has been on dipoles at the interfaces of dielectrics, which have permittivity

greater than vacuum, $\epsilon_r > 1$. In this work and our related work [28] however, we aim to systematically study the radiation pattern of a dipole at the interface of an air-metamaterial (MTM), in which the metamaterial is a homogenized medium with an effective permittivity lower than free space, $\epsilon < \epsilon_0$. Such materials would be classified as Epsilon Near Zero (ENZ) media. One motivation here is to obtain the interesting dielectric-side radiation patterns of [9, 11, 12] in air. The argument for using ENZ is simple. By using an ENZ instead of the dielectric, air plays the role of the dielectric in [12]. Therefore those patterns obtained inside the dielectric in [9, 11, 12], should be attainable now in the air side, as air now acts as the higher permittivity medium compared to the MTM. Aside from the shape, the intensity of the radiation is also stronger in air, rather than in the ENZ. This is for instance very desirable in telecommunication applications. We further generalize the problem to that of a dipole above an 'anisotropic medium', with potentially low value(s) in the permittivity tensor. Since most ENZ media are realized with layered or wire medium type structures, the resulting effective medium is inherently anisotropic and typically similar to a uniaxial crystal with a well defined optical axis.

A simple approach for determining the radiation pattern is using the Lorentz Reciprocity Theorem, which has usually been used for finding the radiation pattern of dipoles on isotropic dielectrics [12]. In this work and [28] we utilize the reciprocity method for systematically studying the dipole radiation above an anisotropic half-space, which is potentially an ENZ medium. We expand the theory to solve for dipoles immersed inside an ENZ medium. Realizations of ENZs are usually anisotropic, that is the near zero permittivity is achieved only along one axis, e.g., using layered media. Based on the pioneering work of Collin on artificial dielectrics [29, 30], the ENZs in this work are realized by interleaving layers of metal and dielectric with a sub-wavelength period. In [29] Collin showed that such a periodic structure can be homogenized into an effective medium with an anisotropic (uniaxial) permittivity tensor and derived simple expressions which have been rediscovered and used extensively to date. In this work, the ENZ realizations are tailored for optical frequencies where it can enable various applications for better light emission, such as shaping the radiation of optical antennas or enhancing the radiation of fluorescent molecules. Both elliptic and hyperbolic anisotropic ENZ media are considered and the subtle differences between the corresponding far field patterns are highlighted.

A related scenario to our problem of interest is the work of [31], which utilizes a source immersed in a low permittivity MTM to achieve highly directive emission at microwaves. The structure was realized

using a mesh grid, operating just above the plasma frequency resulting in $0 < \epsilon_r < 1$. In [31] however the source was fully immersed in the MTM. The propagating waves from the source inside the ENZ reach the interface and refract close to normal in air due to Snell's law. Therefore a highly directive beam is emitted in air. The work in [31] was demonstrated at microwaves, but such a scenario has potential at optical frequencies. Our work extends to the case of fully immersed sources such as the scenario in [31] and shows potential realizations at optical frequencies that enhances the radiation of the source in air. In this effort, the distinct difference between the patterns from interfacial and immersed dipoles is investigated.

2. THEORY

Consider Figure 1, where a dipole is radiating at the interface of air and a medium with an arbitrary permittivity tensor. We utilize the Lorentz reciprocity method as done in [12], showing that such analysis is applicable to general anisotropic media as well. According to the reciprocity method, in order to find the radiated field E_1 due to the dipole current I_1, one can find the field E_2 due to the far zone dipole current I_2. As long as the two currents are equal, so will be the tangential components of the field.

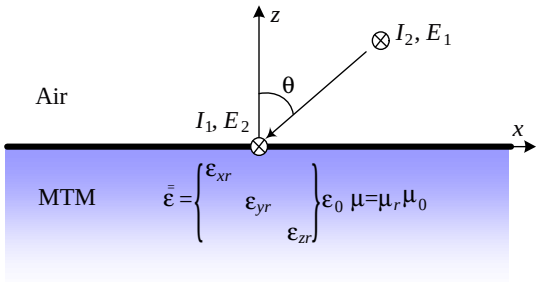

Figure 1. Dipole at the interface of air and anisotropic metamaterial.

We are therefore solving the reciprocal problem, that is finding E_2 which is the total field at the interface when I_2 is radiating. The field from I_2 is a spherical wave of the form $e^{-jkr}/4\pi r$. For a source I_2 in the far-zone, the wave from I_2 incident on the interface can be approximated as a plane wave $E_i(\theta)$. As shown in Figure 2(a), under plane-wave illumination the field at the interface is equal to the field just below the interface. The total field just below the interface is equal to $\tau(\theta)E_i(\theta)$, i.e., the incident field multiplied by the transmission coefficient going from air to the MTM. The problem

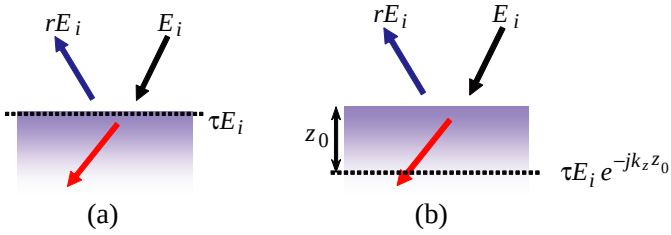

Figure 2. Transmission and reflection from an MTM half-space, (a) at the interface, (b) at a distance z_0 below the interface.

therefore reduces to finding the Fresnel transmission coefficient $\tau(\theta)$ of an oblique incident plane wave on the interface of a general anisotropic medium, under both polarizations. This is arguably an easier problem to solve than other techniques, hence the reason the reciprocity method is a powerful and simple method especially for finding far-zone radiated fields. Once $E_2(\theta)$ is found from this reciprocal scenario, we have essentially determined the desired radiation pattern of I_1 in transmit mode. We only need to multiply by the free space angular pattern of the radiating element I_1 (if any) to find out the overall transmit mode pattern we originally desired.

2.1. Plane-wave Incidence

The Fresnel reflection and transmission coefficients for an interface between air and a uniaxial crystal is found by enforcing the boundary condition for the continuity of the tangential fields at the interface. One can formulate the expressions based only on the incident angle from air, θ. For example in the x-z plane of incidence, the reflection coefficient for the TM (Transverse Magnetic) or p-polarization is

$$r_{\mathrm{TM}} = \frac{\cos\theta - \sqrt{(\mu_r/\epsilon_{xr} - \sin^2\theta/\epsilon_{zr}\epsilon_{xr})}}{\cos\theta + \sqrt{(\mu_r/\epsilon_{xr} - \sin^2\theta/\epsilon_{zr}\epsilon_{xr})}} \tag{1}$$

and for the TE (Transverse Electric) or s-polarization is

$$r_{\mathrm{TE}} = \frac{\cos\theta - \sqrt{\mu_r\epsilon_{yr} - \sin^2\theta}}{\cos\theta + \sqrt{\mu_r\epsilon_{yr} - \sin^2\theta}} \tag{2}$$

The expressions presented in this form are applicable to any half-space that is an anisotropic medium, with arbitrary permittivity along its different axes.

The main cases of interest in this work are anisotropic ENZs, i.e., media where the permittivity is close to zero, at least along one axis. For TE polarization, the out-of-plane permittivity is only relevant and can be close to zero. In TM polarization, two permittivity values (longitudinal and transverse) are relevant. Either of these two permittivity values can be close to zero, and either can be positive or negative, in general. Therefore there are eight dispersion cases for this polarization, with $\{\epsilon_{xr} \to 0^{\pm}, \epsilon_{zr} = \pm 1\}$ or $\{\epsilon_{xr} \to \pm 1, \epsilon_{zr} \to 0^{\pm}\}$. As will be explained later, in this work we are primarily interested in the scenarios with low longitudinal permittivity ($\epsilon_{zr} \to 0^{\pm}$). Three of these scenarios lead to propagation inside the ENZ which will be used here.

Figure 3(a) shows the magnitude of the TM reflection coefficient

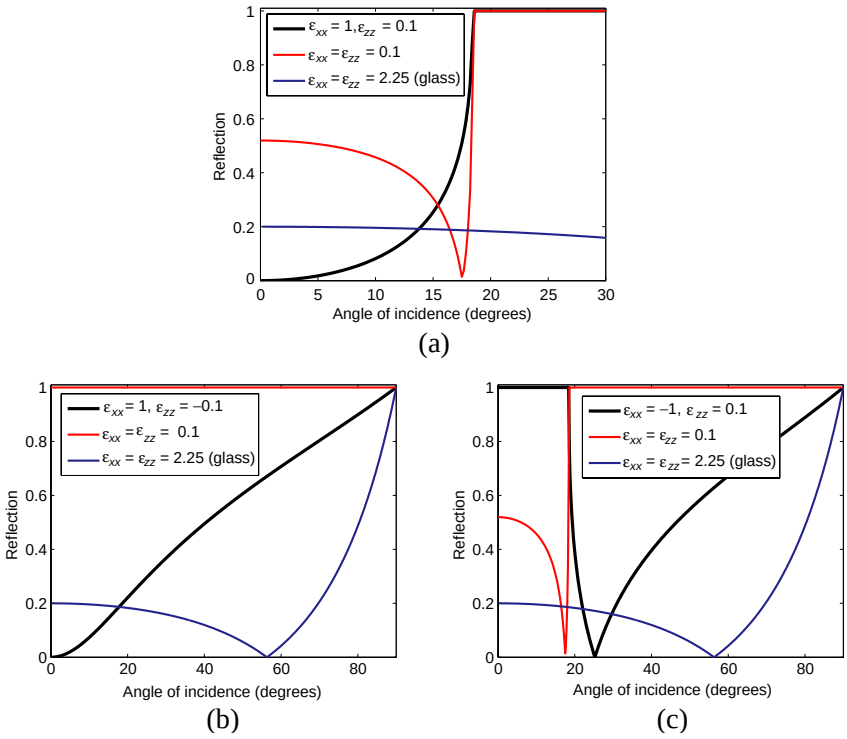

Figure 3. (a) Iso-frequency contours for refraction at the interface of an ENZ with $\epsilon_{xr} = 0.1$, $\epsilon_{zr} = 1$ and air. (b) Reflection coefficient at the interface of air and an anisotropic ENZ with $\epsilon_{zr} = 0.1$, $\epsilon_{xr} = 1$ compared to the reflection from an isotropic MTM with $\epsilon_r = 0.1$.

at the interface of an anisotropic ENZ with $\epsilon_{zr} = 0.1$, $\epsilon_{xr} = 1$ (black curve). It also compares it to the reflection from an isotropic ENZ with $\epsilon_r = 0.1$ (red curve). The figure shows that the reflection is lower in the anisotropic case, for all angles below 15°, compared to the isotropic ENZ of the same low permittivity. It also shows that the two media only accept plane waves that are incident up to a critical angle equal to $\sin^{-1}\sqrt{\epsilon_{zr}}$. Beyond the critical angle the reflection coefficient going from air (dense medium) to the ENZ is 1 as the incident wave experiences Total Internal Reflection (TIR) back into air. Hence for any angle beyond the critical angle up to 90° the transmitted wave into the ENZ is an evanescent wave (only showing up to 30° for illustration purposes). There is also no Brewster's angle (angle at which reflection is zero) for the anisotropic case, while in the isotropic ENZ case there exists a zero reflection angle of incidence close to the critical angle under the TM (p-polarization). For comparison, reflection from a typical dielectric such as glass (blue curve) is also shown.

Figure 4(a) shows the corresponding iso-frequency contour and refraction at the interface of air and the anisotropic ENZ with $\{\epsilon_{xr} = 1, \epsilon_{zr} = 0.1\}$. Such a medium has an elliptic iso-frequency curve as shown in the figure. An incident wave from air, phase matches at the interface to another wave with equal lateral wave-number k_x in the ENZ. The wave-vector in the ENZ is the vector joining the origin to the corresponding point on the elliptical iso-frequency contour. The direction of power flow (Poynting vector) is normal to the iso-frequency

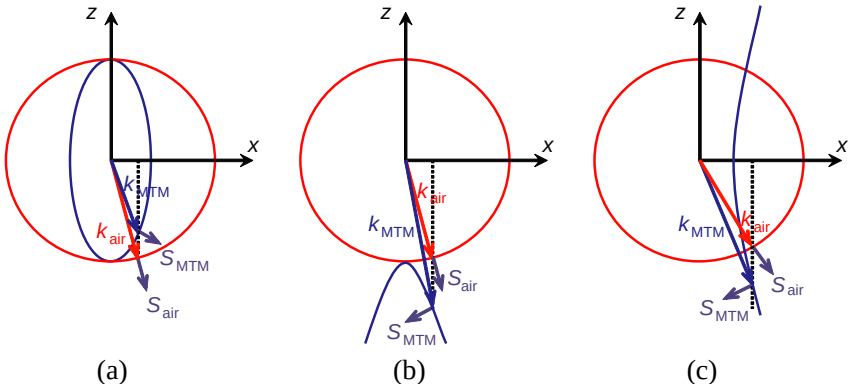

Figure 4. Iso-frequency contour showing wave-vectors and Poynting vector for the interface of air and half-space ENZ with (a) elliptic $\{\epsilon_{xr} = +1, \epsilon_{xr} = +0.1\}$, (b) hyperbolic $\{\epsilon_{xr} = +1, \epsilon_{xr} = -0.1\}$, and (c) hyperbolic $\{\epsilon_{xr} = -1, \epsilon_{xr} = +0.1\}$ characteristic.

contour at any given point as indicated in Figure 3(a). Although the power flows in the direction of the wave-vector (and hence phase velocity) in air, the power flow inside the ENZ is at an angle with respect to the phase velocity due to the anisotropy.

If the signs of the two in-plane permittivity values agree, the iso-frequency contour is elliptic and if they are of opposite signs, the iso-frequency contour is hyperbolic giving rise to a hyperbolic metamaterial (as in the hyperlens [32–34]). Two additional hyperbolic cases with low longitudinal permittivity $\{\epsilon_{xr} \to \pm 1,\ \epsilon_{zr} \to 0^{\mp}\}$ are shown in Figures 4(b) and (c), showing refraction in each case. In the case of Figure 4(b), $\{\epsilon_{xr} = +1,\ \epsilon_{zr} = -0.1\}$, the medium is an indefinite medium. The magnitude of the reflection coefficient from this medium as a function of the incident angle is shown in Figure 3(b). We see that there is no critical angle in this case for all incident angles from air such that the wave never experiences TIR back into air. The amount of reflection coefficient increases gradually with the incident angle in an almost linear trend. Reflection from a typical dielectric such as glass (blue curve) is also shown which has a Brewester's angle at 56.3° in this polarization.

In the case of Figure 4(c), $\{\epsilon_{xr} = -1, \epsilon_{zr} = +0.1\}$, we have another hyperbolic ENZ with low longitudinal permittivity where the medium acts somewhat strangely in terms of Total Internal Reflection. What is surprising in this case is that for all incident angles from broadside up to a critical angle $\theta'_c = \sin^{-1}\sqrt{\epsilon_{zr}}$, the wave experiences TIR back into air because there is no allowed propagation in the ENZ. For all incident angles beyond that critical angle the wave phase matches to a propagating wave in the ENZ. This type of operation is quite the opposite of typical TIR in dielectrics (and even the elliptic ENZ), where in fact the TIR occurs for angles beyond the critical angle. This is also evident when inspecting the reflection coefficient in Figure 3(c). We see that the reflection magnitude for this ENZ (black curve) is 1 for all angles up to θ'_c (i.e., there is TIR back into air for angles close to broadside), while there is transmission into the ENZ for all angles above the critical angle with gradual increase in the reflection coefficient magnitude.

2.2. Interfacial Dipoles

Using the expressions obtained thus far we can find the radiation patterns of a horizontal dipole placed at the interface of the two media. Depending on the orientation of the dipole relative to the anisotropic MTM, different polarization planes are realized. Here we are primarily interested in the principal planes which are the planes containing the principal axes of the MTM. Moreover, we are interested in the cases

where the dipole is oriented along one of these major axes. Figure 5 shows the four primary polarization planes for the horizontal dipole above the anisotropic MTM.

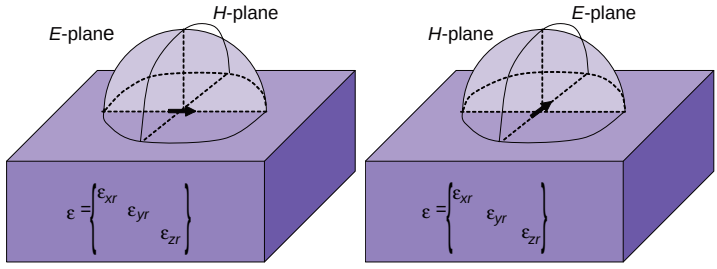

Figure 5. Four principal polarization planes for a dipole oriented along the principal axes of an anisotropic MTM.

Given the chosen geometry of Figure 1 and the previously discussed reciprocity method, the radiation pattern for an interfacial x-directed dipole in the x-z plane is found to be

$$S_{E\text{-plane}}(\theta) = \left[\frac{\cos\theta\sqrt{\mu_r - \sin^2\theta/\epsilon_{zr}}}{\cos\theta\sqrt{\epsilon_{xr}} + \sqrt{\mu_r - \sin^2\theta/\epsilon_{zr}}}\right]^2 \tag{3}$$

for the E-plane (E field in the x-z plane). The $\cos\theta$ term in the numerator is due to the element pattern of a horizontal dipole in free space. The H-plane of such scenario is the y-z plane and the pattern is:

$$S_{H\text{-plane}}(\theta) = \left[\frac{\mu_r\cos\theta}{\mu_r\cos\theta + \sqrt{\mu_r\epsilon_{xr} - \sin^2\theta}}\right]^2. \tag{4}$$

For a y-directed dipole (i.e., current out of x-z plane), the x-z plane is the H-plane and the radiation pattern (E_y only) is

$$S_{H\text{-plane}}(\theta) = \left[\frac{\mu_r\cos\theta}{\mu_r\cos\theta + \sqrt{\mu_r\epsilon_{yr} - \sin^2\theta}}\right]^2. \tag{5}$$

whereas the y-z plane is the E-plane and the radiation pattern is

$$S_{E\text{-plane}}(\theta) = \left[\frac{\cos\theta\sqrt{\mu_r - \sin^2\theta/\epsilon_{zr}}}{\cos\theta\sqrt{\epsilon_{yr}} + \sqrt{\mu_r - \sin^2\theta/\epsilon_{yr}}}\right]^2 \tag{6}$$

This formulation now allows for the relative permittivity ϵ_{xr}, ϵ_{yr} or ϵ_{zr} to be of different values and potentially less than 1. A similar analysis may be applied to media with an anisotropic permeability tensor.

The theory assumes that the homogeneous MTM medium is an infinite half space with no bounds and reflections. Such a scenario may be attainable in practice by using a large enough medium, terminated with another matched medium or with absorbers.

2.3. Immersed Dipole in an ENZ

We can also extend the theory to account for the source buried below the interface of the MTM at a distance z_0 below the surface. Revisiting the reciprocity solution, in the reciprocal problem, the transmitted wave $\tau(\theta)E_i(\theta)$ now travels an extra longitudinal distance of z_0 before reaching the source plane, as depicted in Figure 2(b). Hence this wave needs to be multiplied by an $e^{-jk_z z_0}$ propagation factor. Moreover, this propagation occurs inside the anisotropic MTM. For instance in the x-z plane, the propagation inside an anisotropic crystal for the TM case is described by

$$k_x^2/\epsilon_{zr} + k_z^2/\epsilon_{xr} = k_0^2 \tag{7}$$

and for the TE case it is governed by

$$k_x^2 + k_z^2 = \epsilon_{yr} k_0^2 \tag{8}$$

The transmitted wave just below the interface phase matches such that it has a transverse wave-number component equal to that of the incident wave, $k_x = k_0 \sin\theta$. Therefore the longitudinal component of the wavenumber is found from (7) or (8). The overall pattern of the immersed dipole can be therefore approximated as

$$S_{E\text{-plane}}(\theta)|_{z_0} = e^{-jk_z(\theta)z_0} S_{E\text{-plane}}(\theta)|_0 \tag{9}$$

in the x-z plane for the x-directed dipole and

$$S_{H\text{-plane}}(\theta)|_{z_0} = e^{-jk_z(\theta)z_0} S_{H\text{-plane}}(\theta)|_0 \tag{10}$$

in the x-z plane for the y-directed dipole.

A note of interest is that this additional exponential phase term can become an attenuation factor. In fact, for all angles of incidence from air above the critical angle, the wave phase matches to an evanescent wave in the ENZ (due to TIR in air) which is characterized by an exponentially decaying factor, $e^{-|k_z|z_0}$. As we shall see, in the transmit mode where the dipole is radiating from within the ENZ, a sufficiently distant source from the interface can lead to directive single lobe radiation explaining the observations reported in [31].

3. RADIATION PATTERNS

3.1. Dipole on an Isotropic ENZ

Using the derived radiation patterns for general anisotropic half-space, we can inspect radiation from both isotropic and anisotropic ENZ half-spaces. As a first example we inspect the radiation pattern of a dipole at the interface of an isotropic ENZ as shown in Figure 6. The ENZ is chosen to have a relative permittivity of $\epsilon_{xr} = \epsilon_{yr} = \epsilon_{zr} = 0.1$. It can be seen that these radiation patterns closely resemble the radiation patterns that are typically attained inside dielectrics reported in various works such as [9, 11–13]. However, these radiation patterns behave oppositely to the dielectric half-space scenario, as air is now the denser medium compared to the ENZ. This means that a critical angle occurs in air relative to the ENZ. We are primarily interested in the radiation pattern in the air-side.

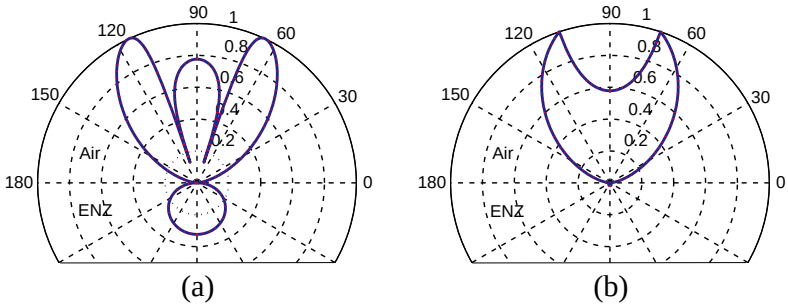

Figure 6. (a) E-plane pattern and (b) H-plane pattern of a dipole at the interface of an isotropic MTM with $\epsilon_r = 0.1$, from [28].

The E-plane pattern has three lobes, a broadside lobe and two side-lobes beyond the critical angle of air. Another important consequence of air being the denser medium is that that the amount of radiated power is also much stronger in the air-side. This is the reverse of the case of the dielectric half-space, where most power radiates into the dielectric side. The H-plane pattern also exhibits the pointed radiation patterns that are typically attained in the H-plane pattern of the dielectric half-space (e.g., see [9, 11–13]). The radiation in the ENZ side is significantly weaker than in air as seen in the H-plane pattern.

3.2. Interfacial Dipole on an Anisotropic ENZ

As stated earlier, ENZs are usually anisotropic in practice. The derived radiation patterns can handle such anisotropy for different orientations of the dipole.

In H-plane, only the out-of-plane permittivity is relevant. Figure 7 shows the H-plane radiation patterns for four values of $0 < \epsilon_{yr} < 1$, for a y-directed dipole. It can be seen that the angles at which the two peaks occur in the pattern (which is determined by the critical angle in air), separate further for larger permittivity values.

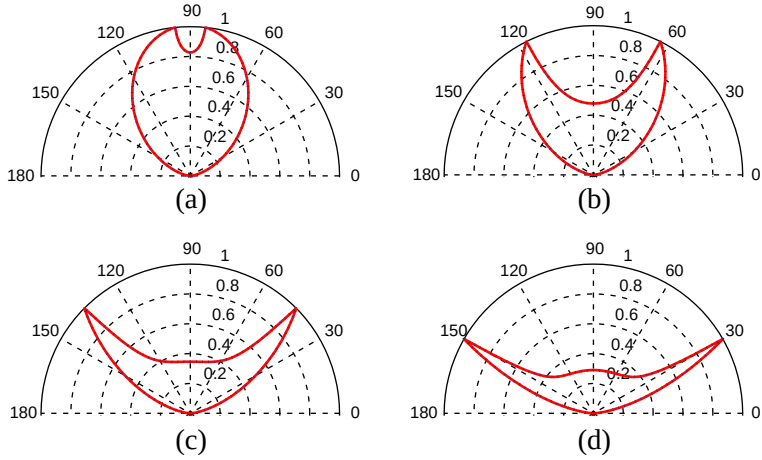

Figure 7. H-plane radiation pattern in air. (a) $\epsilon_{yr} = 0.01$, (b) $\epsilon_{yr} = 0.2$, (c) $\epsilon_{yr} = 0.5$, (d) $\epsilon_{yr} = 0.7$, from [28].

In the E-plane the anisotropy affects the patterns with two permittivity values (transverse and longitudinal), as apparent in the pattern expressions (3) and (6). The four cases of low transverse permittivity, i.e., $\{\epsilon_{xr} \to \pm 0$ and $\epsilon_{zr} = \pm 1\}$, do not lead to similarly shaped E-plane radiation patterns but they rather yield a single lobe. The requirement is then to have a low longitudinal permittivity in order to achieve the E-plane dielectric-side radiation patterns of [9, 11–13] in air, using an ENZ. Therefore for the scope of this paper, we primarily investigate low transverse permittivity cases.

Figure 8 (solid blue curves) shows the E-plane radiation patterns for four values of the longitudinal permittivity $0 < \epsilon_{zr} < 1$, while the transverse permittivity is $\epsilon_{xr} = \epsilon_{yr} = 1$, for a x-directed dipole. Each plot also contains a second trace (dashed red) showing the E-plane radiation pattern if the ENZ were isotropic with the corresponding relative permittivity $\epsilon_r = \epsilon_{zr}$. We can see from these results that

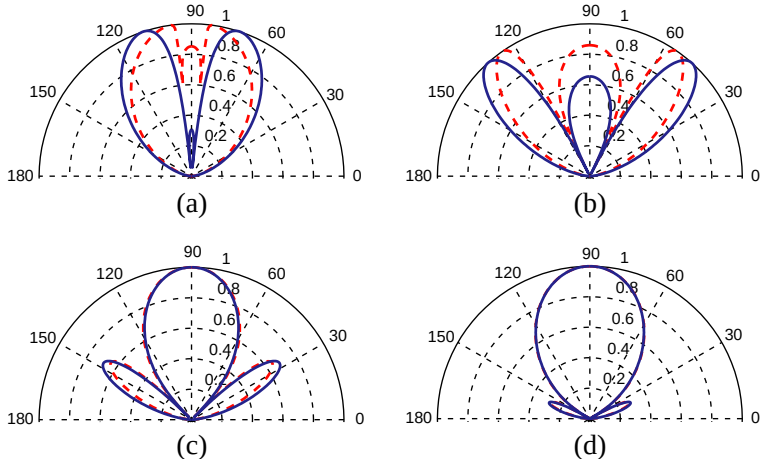

Figure 8. E-plane radiation pattern in air for a dipole above an anisotropic ENZ (solid blue curve) with $\epsilon_{xr} = \epsilon_{yr} = 1$, (a) $\epsilon_{zr} = 0.01$, (b) $\epsilon_{zr} = 0.2$, (c) $\epsilon_{zr} = 0.5$, (d) $\epsilon_{zr} = 0.7$, and (dashed red curve) for the corresponding isotropic ENZ $\epsilon_r = \epsilon_{zr}$, from [28].

similarly shaped radiation patterns can be attained in air even in the presence of this large anisotropy. This is particularly applicable to practical ENZ scenarios that exhibit large anisotropy, as shown later.

The E-plane radiation patterns for the hyperbolic ENZ case of Figure 4(b) are shown in Figure 9, for varying values of $-1 < \epsilon_{zr} < 0$, while $\epsilon_{xr} = 1$. The patterns in this case do not have three lobes and nulls as in Figure 8, rather two merged lobes (without separating nulls) exist in the pattern and there is no main broadside lobe. The lack of nulls (and hence lack of distinct lobes) is due to the absence of a critical angle and no TIR into air for this type of hyperbolic ENZ (in order for the incident and reflected waves to cancel at the interface in the reciprocal problem). The two lobes merge further together into a single lobe as $\epsilon_{zr} \to -1$.

The E-plane radiation patterns for the hyperbolic ENZ case of Figure 4(c) are shown in Figure 10, for varying values of $0 < \epsilon_{zr} < 1$, while $\epsilon_{xr} = -1$. A narrow broadside lobe and two prominent side-lobes exist in the pattern for $\epsilon_{zr} = 0.01$ of Figure 10(a), with distinct separating nulls due to TIR. The two side-lobes reduce in strength relative to the main lobe as $\epsilon_{zr} \to +1$, and the broadside lobe becomes dominant. The two side-lobes diminish more abruptly in this case compared to the corresponding isotropic ENZ case of $\epsilon_r = \epsilon_{zr}$ (dashed red curve).

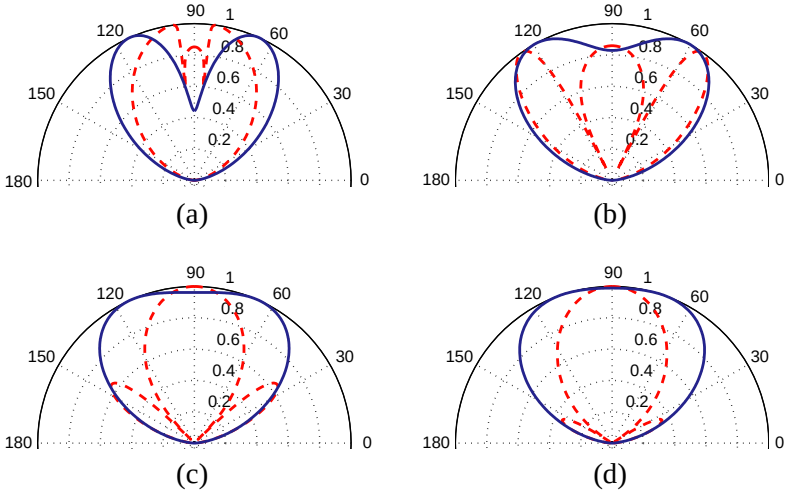

Figure 9. E-plane radiation pattern in air for a dipole above an anisotropic ENZ (solid blue curve) with $\epsilon_{xr} = 1$, (a) $\epsilon_{zr} = -0.01$, (b) $\epsilon_{zr} = -0.2$, (c) $\epsilon_{zr} = -0.5$, (d) $\epsilon_{zr} = -0.7$, and (dashed red curve) for the corresponding isotropic ENZ $\epsilon_r = |\epsilon_{zr}|$.

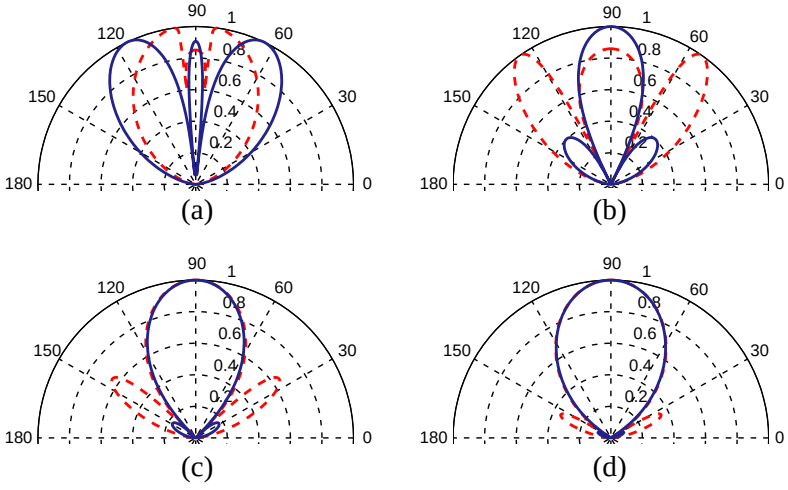

Figure 10. E-plane radiation pattern in air for a dipole above an anisotropic ENZ (solid blue curve) with $\epsilon_{xr} = -1$, (a) $\epsilon_{zr} = 0.01$, (b) $\epsilon_{zr} = 0.2$, (c) $\epsilon_{zr} = 0.5$, (d) $\epsilon_{zr} = 0.7$, and (dashed red curve) for the corresponding isotropic ENZ $\epsilon_r = \epsilon_{zr}$.

3.3. Dipole Immersed in an Anisotropic ENZ

Figure 11 shows the evolution of the radiation pattern in air as an immersed dipole is moved towards the interface (in the case of an elliptical ENZ). Figure 11(a) shows the H-plane pattern of an in-plane dipole, while Figure 11(b) shows the case of E-plane pattern for an out of plane dipole. For the H-plane pattern, it can be seen that when the dipole is fully immersed, a single directive lobe is primarily noticeable in the radiation pattern. As the dipole is moved closer to the interface, the two side-lobes start to emerge. In the case of an interfacial dipole the pattern has two prominent side-lobes and a smaller broadside lobe. The emergence of the side-lobes for interfacial dipoles, as well as those close to the interface, can be attributed to the evanescent near-field waves of the dipole. In such cases, the evanescent waves of the dipole can couple to propagating waves beyond the critical

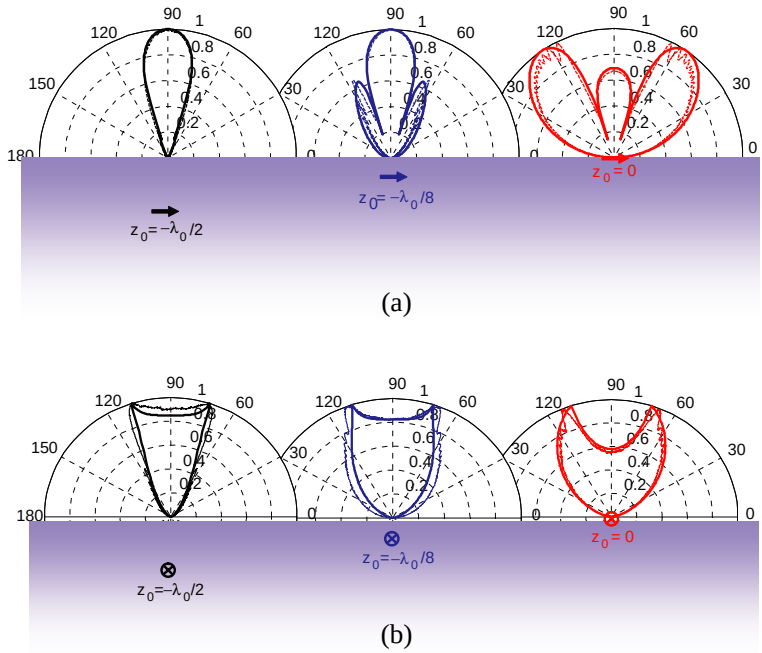

Figure 11. Effect of interfacial versus immersed source in a ENZ MTM. (a) E-plane pattern of an in-plane dipole. (b) H-plane pattern of an out-of-plane dipole. Each graph shows the theoretical far-field pattern using the presented theory (solid curves) and the pattern from fullwave simulation (dashed curves) at a finite observation distance.

angle of air. This is while such evanescent waves become significantly attenuated for larger distances from the interface. Hence in the case of $z_0 = -\lambda_0/2$, there is almost no radiation beyond the critical angle of air with no noticeable side lobes. A similar scenario exists for the E-plane pattern. The pattern for the case of $z_0 = -\lambda_0/2$ has little radiation strength beyond the critical angle with an almost flat-top type radiation pattern. The pattern widens as the dipole moves closer to the interface, such that the familiar pointed radiation patterns of the interfacial case develops. The cases of $z_0 = -\lambda_0/2$ for the two planes essentially recover and explain the scenario of directive emission using ENZs as proposed by [31]. Only the propagating waves of the immersed source reach the surface, all refracting close to normal due to the Snell's law, resulting in a directive broadside lobe.

The two figures also show a secondary dashed curve which is the result of fullwave simulations using a finite size domain for validation purposes. The slight discrepancy and ringing effects in the patterns are well known for finite size simulations and have previously been demonstrated and studied for the dielectric half-space problem [16, 21]. The fullwave simulation results in fact converge to the ideal far-field results for larger observation spheres around the dipole. For instance the results in the two figures are obtained for a radial observation distance of $r_{obs} = 50\lambda_0$. Despite this simulation aberration, it can be seen that the fullwave results confirm the predicted interfacial and immersed far-field patterns.

The immersed dipole results presented here closely resemble the patterns of a dipole above a dielectric [13]. Such patterns were obtained in [13] for the dielectric-side radiation patterns, for varying heights of a source above an isotropic dielectric. The same patterns and trends are now obtained in the air-side, by immersing the dipole inside an elliptic ENZ at different heights.

4. REALIZATION USING ANISOTROPIC ARTIFICIAL DIELECTRICS

The expressions and pattern results presented so far are applicable to general anisotropic media using only the permittivity tensor, independent of the realization of the MTM. Depending on the realization of the MTM, the permittivity tensor may be effectively related to the geometry and material parameters of the underlying unit cells of the actual MTM. The interest in this work has primarily been on ENZs, which may be realized with unit cells such as bi-layers, mesh grids, or wire media depending on the frequency of operation, typically showing some sort of anisotropy. Here we utilize the bi-layer

media at optical frequencies.

Collin showed in [29] that periodic sub-wavelength layers of two dielectrics can be effectively homogenized as one dielectric with an anisotropic uniaxial permittivity tensor, in the investigations related to artificial dielectrics [29, 30]. Such artificial dielectrics were the forerunners to what is now known as a type of Metamaterials.

To date this stacked bi-layer medium has been used in many studies, especially at optical frequencies in the past decade [32–42], primarily due to their simple nature and ease of fabrication. The bi-layer concept has been particularly useful for the realization of Epsilon Near Zero MTMs [36] where the desired "close to zero permittivity" is typically achieved by interleaving sub-wavelength layers of a material with positive permittivity and a material with negative permittivity, such that the effective medium is zero. This was the key for realizing the highly anisotropic ENZs of the hyperlens [32–34], where the effective medium has a hyperbolic dispersion characteristic. Ref. [43] utilized such layered MTMs to propose extreme boundary conditions such as perfect electric and magnetic conductors at optical frequencies and determined the radiation pattern of a dipole near a layered structure that is operating in the theoretical extreme limit $\{\epsilon_{tangential} \to \infty, \epsilon_{normal} \to 0\}$.

The desired anisotropic low permittivity MTMs in this work can also be realized with sub-wavelength layers of a metal (negative real permittivity) and a dielectric at the optical frequency of interest. Two orientations of the layered structure are possible as shown in Figure 12. Primarily, horizontal stacks as in Figure 12(b) have been used in

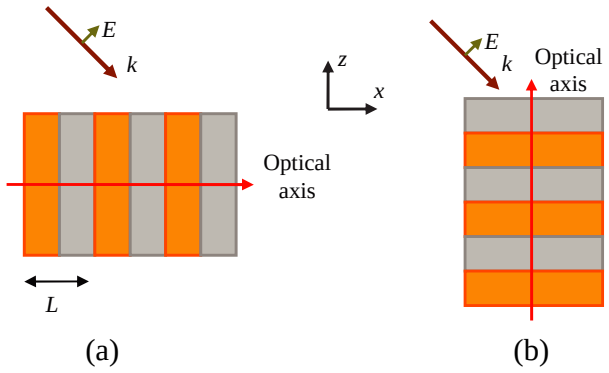

Figure 12. TM light incident on stacked periodic layers realizing an anisotropic medium with two different principal axes having its optical axis oriented along (a) x-axis and (b) z-axis.

the past [32–34] as transverse zero permittivity was required. Here we utilize vertical layers as shown in Figure 12(a), as they offer an advantageous capability for our purposes. The effective permittivity along the two principal axes of such a structure can be found using the following first order Effective Medium Theory (EMT) formulas [29]:

$$\epsilon_{axis} = \frac{\epsilon_m \epsilon_d}{(1-p)\epsilon_m + (p)\epsilon_d} \tag{11}$$

$$\epsilon_{\perp axis} = p\epsilon_m + (1-p)\epsilon_d \tag{12}$$

where ϵ_m and ϵ_d are the permittivity values of the metal and dielectric layers respectively and 'p' is the filling ratio of the metal layer (thickness of the metal layer divided by the sum of the thickness of metal and dielectric layers). A second order effective medium approximation was also presented in [29], however we use the first order formulas to obtain initial values. The period used here is deeply sub-wavelength ($L = \lambda_0/22$) and therefore the second order effects were found not to cause noticeable difference in the effective permittivity values.

We utilize the case of vertical layers to realize zero longitudinal (z-axis) permittivity, mainly due to the fact that close to zero response can be easily achieved along the axis normal to the optical axis with readily available optical materials. A trend of the variation of the complex permittivity as a function of the filling ratio of the metal is shown in Figure 13, utilizing the first order Effective Medium Theory formulas as in [29]. The operation region of interest has been magnified

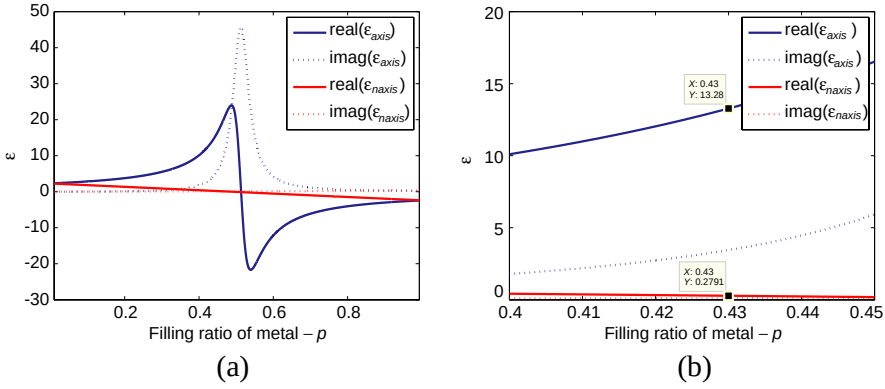

Figure 13. (a) Variation of complex permittivity as a function of metal filling ratio "p" according to EMT expression, using bi-layers of Ag and PMMA at $\lambda_0 = 365\,\text{nm}$. (b) Operation region of interest yielding close to zero anisotropic permittivity with low losses.

in Figure 13(b). The variation is dependent on the choice of the two materials. Here we have used Ag ($\epsilon_m = -2.4012 + 0.2488j$) [34] and PMMA (Polymethyl methacrylate $-\epsilon_d = 2.301$) at $\lambda_0 = 365\,\text{nm}$.

One drawback with using the EMT formulas of [29] is the lack of incorporating additional modes which can arise from rapid field variations compared to the scale of the layers, especially in the optical regime where the metal layer has negative permittivity [37–42]. For example, Surface Plasmon Polaritons can exist when a metal layer with negative permittivity is next to a dielectric [38], creating a non-local response. Such non-local effects are known to give rise to spatial dispersion and have sparked research into providing corrections to the simple EMT model [37–40, 42]. Depending on how sub-wavelength the period is, especially relative to the plasma wavelength, the effective permittivity values obtained from EMT can be significantly different and also dependent on the direction of propagation. This can be better seen by referring to the accurate dispersion equations governing the layered media obtained using the transfer-matrix method for photonic crystals (e.g., see [37, 38, 42]). However, the EMT formulas hold for a variety of angles when the period is sufficiently sub-wavelength (especially when well below the plasma wavelength of the metal layer) and are a good approximate first step when designing layered structures. A benefit of the general pattern expressions presented earlier is that they can be used along with more refined effective permittivity expressions that incorporate nonlocal effects such as [38–40, 42] to arrive at more accurate radiation pattern expressions, if required.

4.1. Radiation from a Finite Slab

The bi-layer structure of Ag and PMMA is tailored at $\lambda_0 = 365\,\text{nm}$ with a filling ratio of $p = 0.43$, and period $L = \lambda_0/22$, which leads to an effective permittivity of $\epsilon_{xr} = 13.27654 + 3.45504j$ and $\epsilon_{zr} = 0.27905 + 0.10698j$ using the EMT expressions. Figures 14 and 15 show the radiation of a horizontal dipole placed at the interface of a finite slab made of such layered structure. The 2D fullwave simulation results presented here are for a 'finite' slab ($6\lambda_0 \times 6\lambda_0 \times 2\lambda_0$) as it is a more practical case to both simulate and potentially fabricate instead of the infinite half-space case.

The inset in Figure 14(a) shows the vertical stacked layers as well as the orientation of the dipole normal to the layers at the interface. The far-field radiation pattern in Figure 14(b) is an E-plane pattern. Three radiation patterns are shown in the figure. The blue curve marks the theoretical patterns for the dipole at the infinite half-space using the theory presented earlier, with the permittivity values obtained from

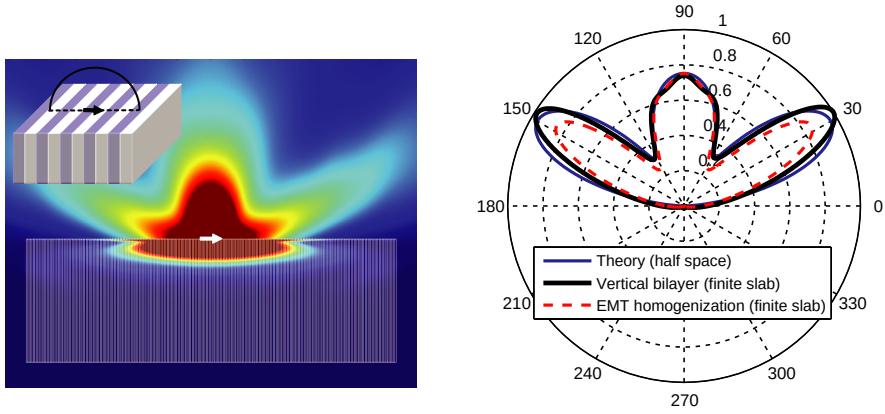

Figure 14. (a) Power density color map of an interfacial horizontal dipole on a slab made of stacked bi-layer of Ag and PMMA at $\lambda_0 = 365\,\text{nm}$. Inset shows the layered slab, dipole orientation normal to the layers, and pattern plane. (b) E-plane radiation pattern for three cases: infinite half-space from theory (blue curve), an EMT homogenized finite slab (red curve) from fullwave simulations, and the vertically layered finite slab (black curve) from fullwave simulations.

the EMT expressions. The black curve shows the radiation pattern of the actual finite slab made of layers of Ag and PMMA obtained from fullwave simulations using the COMSOL 4.3a software package. The dashed red curve shows the pattern from fullwave simulation of a finite slab of the same size, filled with a homogeneous material having permittivity values from the EMT expressions. For the latter two cases, the dipole is placed at a slight distance above the interface in air ($z_0 = 0.009\lambda_0$) due to numerical issues with simulating a fully interfacial case. The discrepancy between the black and red curves is most likely due to a combination of simulation inaccuracies and non-local/spatial dispersion effects. Inaccuracies in simulation of the layered slab (black curve) arise from simulating a large domain with extremely fine plasmonic features, which poses particular challenges as also reported in [38], requiring dense meshing of a large domain. Aside from simulation inaccuracies, a contribution to this discrepancy may be due to non-local effects such that the EMT homogenized slab does not fully capture the complete behavior of the actual layered slab. It should be noted that the slab is illuminated with an adjacent source that has a wide range of spatial frequency components, including propagating

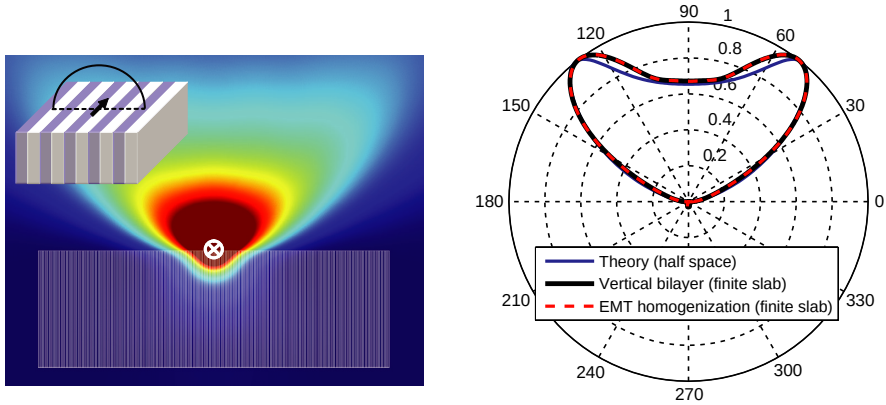

Figure 15. (a) Power density color map of an interfacial horizontal dipole on a slab made of stacked bi-layer of Ag and PMMA at $\lambda_0 = 365\,\text{nm}$. Inset shows the layered slab, dipole orientation parallel to the layers, and pattern plane. (b) H-plane radiation pattern for three cases: infinite half-space from theory (blue curve), an EMT homogenized finite slab (red curve) from fullwave simulations, and the vertically layered finite slab (black curve) from fullwave simulations.

and evanescent waves, exemplifying the potential influence of non-local effects and spatial dispersion (e.g., the excitation of TM SPPs).

Figure 15 shows the scenario of the interfacial dipole parallel to the layers as shown in the inset of power intensity plot of Figure 15(a). Three H-plane radiation patterns are now presented in Figure 15(b). The patterns resemble the H-plane patterns of dielectric with two pointed peaks, with some roundening of the peaks due to losses. This time we see better agreement between the three cases, which shows that the EMT expressions provide a more reliable description of the behavior of the layered slab in the TE polarization than the TM polarization where nonlocal effects are stronger.

From these results, it can be seen that shaped radiation patterns can be achieved in air, by placing the radiator on top of a finite slab of an ENZ realized using the stacked bi-layer structure of [29] at optical frequencies. Such a scenario can enhance the radiated power and tailor the radiation pattern of an optical radiator, e.g., an optical antenna or a florescent molecule for better radiation into far-zone in air. Realizations of the ENZ concept using wire media and mesh grids [31] are also possible for microwave applications.

5. CONCLUSIONS

The radiation of a source at the interface of, or immersed in an anisotropic Epsilon Near Zero (ENZ) Metamaterial is systematically studied. To this end, the radiation patterns of a dipole at or below the interface of air and a general anisotropic MTM half-space are derived using the Lorentz Reciprocity method. It is observed that shaped radiation patterns, which were previously only attained inside dielectrics of high permittivity, are achieved in air by using an ENZ half-space. The intensity of radiation is also much stronger in the air-side, due to role reversal of air as the denser medium. Isotropic ENZs as well as anisotropic ENZs with low longitudinal permittivity were studied for their effect on the radiation pattern in the relevant polarization planes.

In the H-plane, two pointed peaks were observed in the air-side radiation pattern, similar to those obtained in the H-plane patterns of dielectrics. In the E-plane, a dipole on either an isotropic ENZ, an anisotropic elliptic ENZ, or an anisotropic hyperbolic ENZ has two clear nulls in the air-side radiation pattern, as long as the ENZ has *low and positive* longitudinal permittivity. The nulls give rise to a broadside lobe and two side-lobes in air, resembling the E-plane radiation patterns of dielectrics. These pattern features were explained via the reciprocal problem and studying the iso-frequency contours and reflection properties of the ENZ interface under plane wave incidence. It was seen that as long as there is positive low longitudinal permittivity, a critical angle exists in air such that Total Internal Reflection (TIR) occurs back into air for some range of incident angles. The incident field and the totally reflected field cancel out at the interface for an incident angle corresponding to the angle of the null in the pattern of the dipole. The hyperbolic ENZ with low positive longitudinal permittivity showed a peculiar case of TIR *below* the critical angle, which is opposite to that of regular dielectrics. It was also shown that a dipole on a hyperbolic ENZ with *low and negative* longitudinal permittivity has no nulls in the E-plane and only two merged side-lobes. This is because with such an ENZ there is no critical angle in air and TIR does not occur back into air for any incident angle.

The effect of varying the permittivity was shown to affect the critical angle and therefore the patterns in both planes. The effect of immersing the source inside the ENZ was also shown to increase the directivity of the radiation and dampening of off-broadside radiation, both in the H-plane as well as in the E-plane for the isotropic and elliptic ENZ with low longitudinal permittivity. This was due to the occurrence of TIR for all angles above the critical angle in the reciprocal

problem, attenuating the waves that reach the source plane in the ENZ.

Following the pioneering work of Collin, sub-wavelength periodic alternating layers of metals and dielectrics were used for the realization of an anisotropic elliptic ENZ at optical frequencies. It was observed that radiation patterns from a finite slab of such medium in air provides similarly shaped radiation patterns previously only attainable in dielectrics. The presented scenarios have applications in enhancing and shaping the radiation patterns of optical radiators such as optical antennas and fluorescent molecules.

ACKNOWLEDGMENT

The authors thank Prof. Nader Engheta for useful discussions. Financial support from the Natural Sciences and Engineering Research Council of Canada (NSERC) is gratefully acknowledged.

REFERENCES

1. Sommerfeld, A., "Uber die ausbreitung der wellen in der drahtlosen telegraphie," *Annalen der Physik*, Vol. 333, No. 4, 665–736, 1909.
2. Norton, K., "The propagation of radio waves over the surface of the earth and in the upper atmosphere," *Proceedings of the Institute of Radio Engineers*, Vol. 24, No. 10, 1367–1387, 1936.
3. Felsen, L., "Radiation from a uniaxially anisotropic plasma half space," *IEEE Transactions on Antennas and Propagation*, Vol. 11, No. 4, 469–484, 1963.
4. Kong, J., "Electromagnetic fields due to dipole antennas over stratified anisotropic media," *Geophysics*, Vol. 37, No. 6, 985–996, 1972.
5. Lukosz, W. and R. E. Kunz, "Light emission by magnetic and electric dipoles close to a plane interface. I. Total radiated power," *J. Opt. Soc. Am.*, Vol. 67, No. 12, 1607–1615, 1977.
6. Lukosz, W. and R. E. Kunz, "Light emission by magnetic and electric dipoles close to a plane dielectric interface. II. Radiation patterns of perpendicular oriented dipoles," *J. Opt. Soc. Am.*, Vol. 67, No. 12, 1615–1619, 1977.
7. Lukosz, W., "Light emission by magnetic and electric dipoles close to a plane dielectric interface. III. Radiation patterns of dipoles with arbitrary orientation," *J. Opt. Soc. Am.*, Vol. 69, No. 11, 1495–1503, 1979.

8. King, R. and G. Smith, *Antennas in Matter: Fundamentals, Theory and Applications,* MIT Press, Cambridge, MA, 1981.
9. Brewitt-Taylor, C., D. Gunton, and H. Rees, "Planar antennas on a dielectric surface," *Electronics Letters*, Vol. 17, No. 20, 729–731, 1981.
10. Rahmat-Samii, Y., R. Mittra, and P. Parhami, "Evaluation of sommerfeld integrals for lossy half-space problems," *Electromagnetics* Vol. 1, No. 1, 1–28, 1981.
11. Engheta, N., C. H. Papas, and C. Elachi, "Radiation patterns of interfacial dipole antennas," *Radio Science*, Vol. 17, No. 6, 1557–1566, 1982.
12. Rutledge, D. and M. Muha, "Imaging antenna arrays," *IEEE Transactions on Antennas and Propagation*, Vol. 30, No. 4, 535–540, 1982.
13. Smith, G., "Directive properties of antennas for transmission into a material half-space," *IEEE Transactions on Antennas and Propagation*, Vol. 32, No. 3, 232–246, 1984.
14. Engheta, N., C. Papas, and C. Elachi, "Interface extinction and subsurface peaking of the radiation pattern of a line source," *Applied Physics B*, Vol. 26, No. 4, 231–238, 1981.
15. Valle, S., L. Zanzi, M. Sgheiz, G. Lenzi, and J. Friborg, "Ground penetrating radar antennas: Theoretical and experimental directivity functions," *IEEE Transactions on Geoscience and Remote Sensing*, Vol. 39, No. 4, 749–759, 2001.
16. Radzevicius, S. J., C.-C. Chen, L. Peters, Jr., and J. J. Daniels, "Nearfield dipole radiation dynamics through FDTD modeling," *Journal of Applied Geophysics*, Vol. 52, No. 23, 75–91, 2003.
17. Sarabandi, K., M. D. Casciato, and I.-S. Koh, "Efficient calculation of the fields of a dipole radiating above an impedance surface," *IEEE Transactions on Antennas and Propagation*, Vol. 50, No. 9, 1222–1235, 2002.
18. Xu, X.-B. and Y. Huang, "An efficient analysis of vertical dipole antennas above a lossy half-space," *Progress In Electromagnetics Research*, Vol. 74, 353–377, 2007.
19. Firouzeh, Z. H., G. A. Vandenbosch, R. Moini, S. H. H. Sadeghi, and R. Faraji-Dana, "Efficient evaluation of Green's functions for lossy half-space problems," *Progress In Electromagnetics Research*, Vol. 109, 139–157, 2010.
20. Parise, M., "Exact electromagnetic field excited by a vertical magnetic dipole on the surface of a lossy half-space," *Progress In Electromagnetics Research B*, Vol. 23, 69–82, 2010.

21. Luan, L., P. R. Sievert, and J. B. Ketterson, "Near-field and farfield electric dipole radiation in the vicinity of a planar dielectric half space," *New Journal of Physics*, Vol. 8, No. 11, 264, 2006.
22. Felsen, L., "Lateral waves on an anisotropic plasma interface," *IRE Transactions on Antennas and Propagation*, Vol. 10, No. 3, 347–349, 1962.
23. Shavit, R. and E. Rosen, "Lateral wave contribution to the radiation from a dielectric half medium," *IEEE Transactions on Antennas and Propagation*, Vol. 43, No. 7, 751–755, 1995.
24. Rafi, G. Z., R. Moini-Mazandaran, and R. Faraji-Dana, "A new time domain approach for analysis of vertical magnetic dipole radiation in front of lossy half-space," *Progress In Electromagnetics Research*, Vol. 29, 57–68, 2000.
25. Tsalamengas, J. and N. Uzunoglu, "Radiation from a dipole near a general anisotropic layer," *IEEE Transactions on Antennas and Propagation*, Vol. 38, No. 1, 9–16, 1990.
26. Saarinen, J. J. and J. E. Sipe, "A Green function approach to surface optics in anisotropic media," *Journal of Modern Optics*, Vol. 55, No. 1, 13–32, 2008.
27. Alù, A., M. G. Silveirinha, A. Salandrino, and N. Engheta, "Epsilon-near-zero metamaterials and electromagnetic sources: Tailoring the radiation phase pattern," *Phys. Rev. B*, Vol. 75, 155410, 2007.
28. Memarian, M. and G. V. Eleftheriades, "Radiation of dipoles at the interface of low permittivity media," *Proc. IEEE International Symp. on Antennas and Propagation*, 2013.
29. Collin, R. E., "A simple artificial anisotropic dielectric medium," *IRE Transactions on Microwave Theory and Techniques*, Vol. 6, No. 2, 206–209, 1958.
30. Collin, R. E., *Field Theory of Guided Waves,* IEEE Press Series on Electromagnetic Wave Theory, Wiley, 1990.
31. Enoch, S., G. Tayeb, P. Sabouroux, N. Guérin, and P. Vincent, "A metamaterial for directive emission," *Physical Review Letters*, Vol. 89, No. 21, 213902, 2002.
32. Salandrino, A. and N. Engheta, "Far-field subdiffraction optical microscopy using metamaterial crystals: Theory and simulations," *Phys. Rev. B*, Vol. 74, 075103, 2006.
33. Jacob, Z., L. V. Alekseyev, and E. Narimanov, "Optical hyperlens: Far-field imaging beyond the diffraction limit," *Opt. Express*, Vol. 14, No. 18, 8247–8256, 2006.

34. Liu, Z., H. Lee, Y. Xiong, C. Sun, and X. Zhang, "Far-field optical hyperlens magnifying sub-diffraction-limited objects," *Science*, Vol. 315, No. 5819, 1686, 2007.
35. Fang, A., T. Koschny, and C. M. Soukoulis, "Optical anisotropic metamaterials: Negative refraction and focusing," *Phys. Rev. B*, Vol. 79, 245127, 2009.
36. Engheta, N., "Pursuing near-zero response," *Science*, Vol. 340, No. 6130, 286–287, 2013.
37. Elser, J., V. A. Podolskiy, I. Salakhutdinov, and I. Avrutsky, "Nonlocal effects in effective-medium response of nanolayered metamaterials," *Applied Physics Letters*, Vol. 90, No. 19, 191109, 2007.
38. Orlov, A. A., P. M. Voroshilov, P. A. Belov, and Y. S. Kivshar, "Engineered optical nonlocality in nanostructured metamaterials," *Phys. Rev. B*, Vol. 84, 045424, 2011.
39. Chebykin, A. V., A. A. Orlov, A. V. Vozianova, S. I. Maslovski, Y. S. Kivshar, and P. A. Belov, "Nonlocal effective medium model for multilayered metal-dielectric metamaterials," *Phys. Rev. B*, Vol. 84, 115438, 2011.
40. Chebykin, A. V., A. A. Orlov, C. R. Simovski, Y. S. Kivshar, and P. A. Belov, "Nonlocal effective parameters of multilayered metaldielectric metamaterials," *Phys. Rev. B*, Vol. 86, 115420, 2012.
41. Naik, G. V., J. Liu, A. V. Kildishev, V. M. Shalaev, and A. Boltasseva, "Demonstration of Al : ZnO as a plasmonic component for near-infrared metamaterials," *Proceedings of the National Academy of Sciences*, Vol. 109, No. 23, 8834–8838, 2012.
42. Chern, R.-L., "Spatial dispersion and nonlocal effective permittivity for periodic layered metamaterials," *Opt. Express*, Vol. 21, No. 14, 16514–16527, 2013.
43. Alù, A. and N. Engheta, "Extremely anisotropic boundary conditions and their optical applications," *Radio Science*, Vol. 46, No. 5, 1–8, 2011.